August 16, 2012

To Executive Editors H.H.G. Savenije, J. Carrera, and M. Sivapalan

To Editor Insa Neuweiler

Hydrology and Earth System Sciences

Re: Revised Manuscript "EXTENDED POWER-LAW SCALING OF HEAVY-TAILED RANDOM FIELDS OR PROCESSES" by Alberto Guadagnini, Monica Riva and Shlomo P. Neuman,

Dear Editors:

We appreciate the efforts you and the reviewers have invested in our manuscript. We are pleased to submit a revised version in response the reviewers' insightful comments. Modifications to the original version appear in red font within the revised manuscript.

In response to a suggestion by Reviewer 2 we have changed the title to "EXTENDED POWER-LAW SCALING OF HEAVY-TAILED RANDOM AIR-PERMEABILITY FIELDS IN FRACTURED AND SEDIMENTARY ROCKS".

The following is an itemized list of reviewers' comments (in italics) and our responses.

Comments by REVIEWER #1

1. The paper presents a scaling analysis via Extended Self-Similarity aimed at investigating the behavior of two sets of log permeability data collected in the field at two different support scales. The data prove to be consistent with sub-Gaussian random fields subordinated to tfBm (truncated fractional Brownian motion); the parameters of the truncated power variograms and subordinators are then derived for the second data set. The paper is fully within the scope of HESS, and of interest to its readership. The analysis relies on a general scaling theory of subordinated tfBm previously developed by the authors; this is properly acknowledged and described in the technical background introducing the different kinds of subordinators. The background section is concise and clear. The data sets are respectively analyzed in Sections 3 and 4; the first deals with 3-D data from Apache Leap Research Site with support scale of 1 m; the second with 2-D data from Escalante, Utah, with a support scale of 0.15 m. Both the practical implementation of the methodology and the results obtained constitute an important and novel contribution. The method adopted and its assumptions are clearly outlined; the conclusions are solid. The title and abstract reflect adequately the contents of the paper. The paper structure, subdivision into sections, and language are sound; the paper cannot be shortened significantly, nor requires extensive editing. The reference section is broad.

We thank the reviewer for his/her positive assessment of our work. We have modified the title as noted earlier.

2. On p. 7390 lines 10-15 the previous analysis on the Arizona data illustrated in Riva et al.

(2012) is cited. In what respect does the analysis presented here differ from the earlier one?

Riva et al. (2012) analyzed the probability distributions of 1-m scale (natural) log k measurements and their increments at the ALRS. Here we analyze structure functions and scaling of the same data using the ESS approach.

3. Section 3 on Arizona data does not present results for all parameters of the tfBm (e.g. upper and lower cutoffs) as does Section 4 for Utah data. These could be of interest to the reader, in view of the relationship between domain scale and upper cutoff.

These parameter estimates, reported in Riva et al. (2012), are λ_l = 0.48 m and λ_u = 9.98 m. We prefer not to repeat these estimates in the revised HESS manuscript.

4. On p. 7393 lines 4-9 the authors comment on the vertical data at the Utah site, and present results only for horizontal transects D and H. Do the result of the scaling analysis on the omnidirectional data differ significantly from those presented? Does this give any hint on the applicability of the analysis to 3-D data as compared to 1-D ones?

Please see our response to Comment 5 of Reviewer 2 below.

5. In the analysis of the horizontal data at the Utah site, are the two transects analyzed jointly, i.e. M=2 and N=133-136 in (12)?

Yes, in the original manuscript $M=2$. In the revised manuscript M = 2 when analyzing data along transects D and H and M = 3 when analyzing data along transects D, H and X. N varies with lag.

6. Please check for consistency or typos the following sentences: - p. 7389 line 10 replace "are" with "is".

Done.

Comments by the REVIEWER #2

1. The reviewed paper is aimed at the analysis of the scaling behavior of two log permeability data sets from pneumatic air injection tests, which were conducted (a) in six boreholes drilled in unsaturated fractured tuff at the University of Arizona Apache Leap Research Site (ALRS) near Superior, Arizona, and (b) along the two horizontal transects on the outcrop of lower shoreface bioturbated sandstone near Escalante, Utah. These two sites represent two different subsurface environments – unsaturated fractured tuff, and sediments that were impacted by depositional and biological processes.The authors clearly demonstrated that the data sets from both sites showed heavy-tailed frequency distributions, which are consistent with sub-Gaussian random fields subordinated to tfBm, as well as provided maximum likelihood estimates of parameters characterizing the corresponding Lévy stable subordinators and tfBm functions. The paper fully corresponds to the scope of HESS, and would be of interest to its readers involved in the statistical analysis of field permeability tests.

We thank the reviewer for his/her positive assessment of our work.

2. The authors refer to "the heavy-tailed frequency distributions in three and two spatial dimensions," which were obtained at the two sites. It is the opinion of this reviewer that the notion of the three and two spatial dimensions is not clearly presented in the reviewed paper. It seems that the authors refer to different types of experiments at the field sites – 3D configuration of injection intervals in slanted and vertical boreholes at the ALRS, and the 2D transects at the Utah outcrop. It is apparent that the real air-flow dimensions resulting from pneumatic tests were not determined; it could be 2D, 3D, or fractional-dimension flow (e.g., Marechal et al., 2004, Chakrabarty, 1994; Chang et al., 2011).

As stated in the Abstract and the Introduction, "we analyze the scaling behaviors of two field-scale log permeability data sets showing heavy-tailed frequency distributions in three and two spatial dimensions, respectively." By this we mean that, in the first case, local log permeability measurements are distributed throughout a three-dimensional volume of rock and, in the second case, they are distributed along a two-dimensional planar outcrop.

The dimensionality of local flow regimes developing during 1-m scale pneumatic packer tests in unsaturated fractured tuff at the ALRS was analyzed by Illman and Neuman (2000). The authors found that airflow in the vicinity of most such test intervals is three-dimensional, taking place within a locally interconnected set of fractures. Only in a few cases is the flow locally two-dimensional, taking place within a single dominant fracture that intersects the test interval.

We suspect, but are of course not sure, that the same may apply to mini-permeameter data along the Utah outcrop.

Reference

Illman WA and Neuman, SP (2000) Type-curve Interpretation of Multirate Single-Hole Pneumatic Injection Tests in Unsaturated Fractured Rock, 38, 6, 899-911, Ground Water.

3. The analysis of the air permeability tests from the ALRS continues a series of publications stemming from a series single-hole and cross-hole pneumatic injection tests, which were conducted the ALRS. On Page 11, the authors indicate that their analysis is based on the log k values obtained by Guzman et al. (1996) from steady-state interpretation of 184 pneumatic injection tests in 1-m long intervals along 6 boreholes. However, Neuman et al. (2001) indicated that over 270 single-hole tests were conducted in 6 vertical and inclined boreholes at the site by Guzman et al. (1996). Did the authors of the reviewed paper use a subset of tests conducted Guzman et al. (1996)? .

As explained by Illman and Neuman (2000), the 270 packer tests included injection intervals of lengths 0.5, 1, 2 and 3 m. To avoid mixing data measured on disparate scales we focus in this paper exclusively on 184 measurements within test intervals of length 1 m.

4. Neuman et al. (2001) showed that at the ALRS the air permeability values represented directional values. They also showed that k derived from cross-hole tests were much higher than *those from the smaller-scale single-hole tests. In other papers, a pronounced k scale effect was determined from single- and cross-borehole pneumatic injection tests (for example, Illman and Neuman, 2001, 2003; Vesselinov et al., 2001; Neuman and Di Federico, 2003). Illman (2004) suggested that air permeability tests in single boreholes with limited fracture connectivity near the injection interval exhibited 2D flow, while cross-hole tests involved 3D air flow within a highly connective fracture network.*

All ALRS permeabilities analyzed in this paper were derived from single-hole pneumatic packer tests. These local permeabilities contain no directional information and are therefore treated as scalars.

During cross-hole pressure tests at the ALRS (which we are not considering in the present HESS paper) pressure signals travelling along directional paths between injection and monitoring intervals allow one in principle to derive corresponding directional permeabilities on scales proportional to the length of each path. Such directional permeabilities, however, no longer represent local values of the kind we consider in this paper, and are therefore not relevant to our analysis.

Cross-hole tests at the ALRS were analyzed in two ways: (a) tomographically, yielding three-dimensional distributions of permeabilities on a grid of many cells measuring 1 cubic meter each, and (b) by treating the rock covered by this grid as if it was uniform. The first approach yielded permeabilities that are comparable in the mean to those obtained independently from 1-m scale single-hole packer tests. The second approach yielded much larger mean uniform equivalent permeabilities across the entire grid. Since our present analysis deals only with 1-m scale data, this scale effect does not affect it.

The issue of local flow dimensionality was addressed in our response to Comment 2.

5. For the Utah outcrop test, the authors analyzed permeability measurements, which were taken from the two lower transects, and found (Page 14) that the data collected along the vertical profiles were poorly suited for an analysis of vertical log permeability scaling. It would be useful for a reader to explain why the conclusions of the reviewed paper cannot be used for vertical direction at this site. Note that in their paper, Castle et al. (2004) indicated that fractal-based statistical analysis of the horizontal log k increments yielded nearly identical results for both the bioturbated facies and the cross-bedded facies, possibly suggesting an underlying statistical commonality in the formation of both facies. Also, Castle et al. (2010) analyzed the data from the lower portions of the vertical wells in association with the data from the horizontal transects, but the authors of the reviewed paper did not use these data. On Page 14 of the reviewed paper, the authors referred to the total number of measurements (515) collected along the vertical and horizontal cross-sections, while they analyzed only the data along two horizontal transects.

Our revised manuscript now states the following: "Castle et al. (2004) found that whereas sample statistics of (natural) log permeability, log k, vary depending on which facies are considered, the frequency distributions of horizontal log k increments in the two facies are similar. Lu et al. (2002) used a fBm model to generate log k increments within a mix of distinct facies. They showed that, when data from different facies are jointly analyzed, the simulated log k increments exhibit an apparent non-Gaussian distribution. They concluded that observed Lévy-like behavior of sample probability distributions of permeability data can in some cases be an artifact stemming from mixing data associated with different facies. Accordingly, Moltz et al. (2007) focused their analysis on increments along horizontal transects D and H (Fig. 8) within the lower bioturbated facies. They found the horizontal log *k* increments to be well represented by a fractional Laplace noise model. We note however that this model has no provision for characterizing the log *k* values themselves.

In this paper we analyze the frequency distributions and scaling of log *k* values and their horizontal increments (*a*) along transects D and H within the lower bioturbated facies and (b) jointly along transects D, H and X (Fig. 8) in the two facies. We also attempted to perform a similar analysis of log *k* values and their increments along the four vertical transects at the site but found the corresponding samples too small to yield meaningful statistics."

To elaborate further on this latter point, Figure R1 shows the number of data pairs associated with each vertical lag considering (a) data from both facies and (b) data solely from the lower bioturbated facies. In both cases the number of pairs is too small to yield meaningful statistics of the kind we deal with in our manuscript, especially so when one considers a single facies.

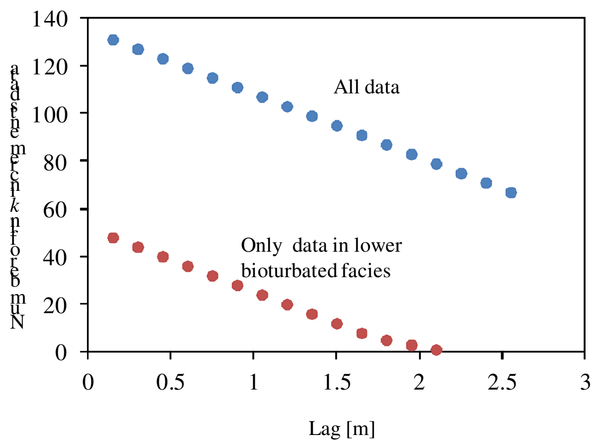

Fig. R1. Number of Utah data pairs associated with each vertical lag.

6. In the list of References (Page 19, lines 368-370), the authors give the title of the paper by Castle et al. (2004) "Sedimentology and facies-dependent permeability,. . ." It was the working title of the paper, and then it was published under the title "Sedimentology and fractal-based analysis of permeability data,. . ." in the Journal – see the citation below.

We thank you the reviewer for pointing out this oversight.

6. In their explanation of the ESS expression (3), the authors refer to the classical case of turbulent velocities with the reference to Chakraborty et al. (2010). It seems it would be important to explain for the readers what is common between turbulent velocities and air permeability tests in fractured rock and sediments.

As noted in our introduction, ESS applies not only to log permeabilities and turbulent velocities but also to a host of other variables such as river morphology, sediment dynamics, financial time series and the like. In this respect, there does not appear to be any special relationship between the first two variables.

7. The paper is entitled, "EXTENDED POWER-LAW SCALING OF HEAVY-TAILED RANDOM FIELDS OR PROCESSES." It is the opinion of this review that this title is too general, and it should be designed to let readers anticipate the content of the paper,which is specifically focused on the analysis of the scaling behavior of air permeability in fractured rock and sediments. For example, "Extended power-law scaling of heavy-tailed random fields of air permeability in fractured porous media."

We changed the title to "EXTENDED POWER-LAW SCALING OF HEAVY-TAILED RANDOM AIR-PERMEABILITY FIELDS IN FRACTURED AND SEDIMENTARY ROCKS."

8. Comments to the figure captions: Fig. 1 – cite the reference to the plot.

Done.

9. Fig. 8. The caption indicates that the figure is modified after Castle et al. (2004). I compared Fig. 8 with the original figure in the paper by Castle et al. and did not see any modification, except a different font of labels. What is modified?

We have redrawn the original figure of Castle et al (2004) by adopting a different frame and symbols to represent measurement locations.

10. *Comment to Fig. 7: Would it be useful to find an analytical expression to describe the computed values given by squares?*

The values in Figure 7 could easily be represented by a polynomial or other analytical expression, but we do not see much purpose in doing so.

Sincerely,

Alberto Guadagnini
D.I.I.A.R. – Politecnico di Milano
Piazza L. Da Vinci, 32
20133 Milano (Italy)
Tel: +39 02 2399 6263
Fax: +39 02 2399 6298
email: alberto.guadagnini@polimi.it

EXTENDED POWER-LAW SCALING OF HEAVY-TAILED RANDOM AIR-PERMEABILITY FIELDS IN FRACTURED AND SEDIMENTARY ROCKS

A. Guadagnini[1], M. Riva[1] and S.P. Neuman[2]

[1]Dipartimento di Ingegneria Idraulica, Ambientale, Infrastrutture Viarie e Rilevamento Politecnico di Milano, Piazza L. Da Vinci 32, 20133 Milano, Italy

[2]Department of Hydrology and Water Resources,
University of Arizona, Tucson, Arizona 85721, USA

ABSTRACT

We analyze the scaling behaviors of two field-scale log permeability data sets showing heavy-tailed frequency distributions in three and two spatial dimensions, respectively. One set consists of 1-m scale pneumatic packer test data from six vertical and inclined boreholes spanning a decameters scale block of unsaturated fractured tuffs near Superior, Arizona, the other of pneumatic minipermeameter data measured at a spacing of 15 cm along three horizontal transects on a 21 m long and 6 m high outcrop of the Upper Cretaceous Straight Cliffs Formation, including lower-shoreface bioturbated and cross-bedded sandstone near Escalante, Utah. Order q sample structure functions of each data set scale as a power $\xi(q)$ of separation scale or lag, s, over limited ranges of s. A procedure known as Extended Self-Similarity (ESS) extends this range to all lags and yields a nonlinear (concave) functional relationship between $\xi(q)$ and q. Whereas the literature tends to associate extended and nonlinear power-law scaling with multifractals or fractional Laplace motions, we have shown elsewhere that (a) ESS of data having a normal frequency distribution is theoretically consistent with (Gaussian) truncated (additive, self-affine, monofractal) fractional Brownian motion (tfBm), the latter being unique in predicting a breakdown in power-law scaling at small and large lags, and (b) nonlinear power-law scaling of data having either normal or heavy-tailed frequency distributions is consistent with samples from sub-Gaussian random fields or processes subordinated to tfBm or truncated fractional Gaussian noise (tfGn), stemming from lack of ergodicity which causes sample moments to scale differently than do their ensemble counterparts. Here we (i) demonstrate that the above two data sets are consistent with sub-Gaussian random fields subordinated to tfBm or tfGn and (ii) provide maximum likelihood estimates of parameters characterizing the corresponding Lévy stable subordinators and tfBm or tfGn functions.

I. INTRODUCTION

Many earth and environmental (as well as physical, ecological, biological and financial) variables exhibit power-law scaling of the following type. Let

$$S_N^q(s) = \frac{1}{N(s)} \sum_{n=1}^{N(s)} \left| \Delta Y_n(s) \right|^q \quad (1)$$

be an order q sample structure function of a random function $Y(\mathbf{x})$ defined on a continuum of points $\mathbf{x}$ in one- or multi-dimensional space (or time), $\Delta Y_n(s) = Y(\mathbf{x}_n + s \cdot \mathbf{m}) - Y(\mathbf{x}_n)$ being a sampled increment of $Y(\mathbf{x})$ over a separation distance (lag) s in one or multiple directions, defined by one or more unit vectors $\mathbf{m}$, between two points and $N(s)$ the number of measured increments. Power-law scaling of $Y(\mathbf{x})$ is described by

$$S_N^q(s) \propto s^{\xi(q)} \quad (2)$$

where the power or scaling exponent, $\xi(q)$, is independent of s. When the scaling exponent is linearly proportional to q, $\xi(q) = Hq$, $Y(\mathbf{x})$ is interpreted to be a self-affine (additive, monofractal) random field (or process) with Hurst exponent H. When $\xi(q)$ varies nonlinearly with q, $Y(\mathbf{x})$ has traditionally been taken to represent multiplicative, multifractal random fields or processes (Neuman, 2010a; Guadagnini et al., 2012). Nonlinear power-law scaling is also exhibited by fractional Laplace motions (Meerschaert et al., 2004; Kozubowski et al., 2006) recently applied to sediment transport data by Ganti et al. (2009).

Power-law scaling is typically assessed by employing the method of moments to analyze samples of measured variables. This entails inferring sample structure functions (1) for a set q_1, q_2, ..., q_n of q values at various lags. The structure function $S_N^{q_i}$ is related to s by linear regression on a log-

log scale, the power $\xi(q_i)$ (i = 1, 2, …, n) being set equal to the slope of the regression line. Linear or near-linear dependence of log $S_N^{q_i}$ on log s is typically limited to intermediate ranges of separation scales, $s_I < s < s_{II}$, outside of which power-law scaling breaks down. The lower and upper limits, s_I and s_{II} respectively, which demarcate the range of power-law scaling are defined theoretically or, in most cases, empirically (Siena et al., 2012; Stumpf and Porter, 2012). Benzi et al. (1993a, 1993b) provided empirical evidence that a procedure they had termed Extended Self-Similarity (ESS) allows widening significantly the range of lags over which velocities in fully developed turbulence (where s_I is taken to be governed by the Kolmogorov's dissipation scale) scale in a manner consistent with (2). Writing (2) as $S^n(s) = C(n)\, s^{\xi(n)}$ and $S^m(s) = C(m)\, s^{\xi(m)}$, solving one of these equations for s and substituting into the other yields the ESS expression

$$S^n(s) \propto S^m(s)^{\beta(n,m)} \tag{3}$$

where $\beta(n,m) = \xi(n)/\xi(m)$ is a ratio of scaling powers. Although the literature does not explain how and why (3) should apply to lags $s < s_I$ and $s > s_{II}$ where power-law scaling (2) breaks down, it nevertheless includes numerous examples demonstrating this to be the case. In addition to the classic case of turbulent velocities (Chakraborty et al., 2010) these examples include geographical (e.g. Earth and Mars topographic profiles), hydraulic (e.g. river morphology and sediment dynamics), atmospheric, astrophysical, (e.g. solar quiescent prominence, low-energy cosmic rays, cosmic microwave background radiation, turbulent boundary layers of the Earth’s magnetosphere), biological (e.g. human heartbeat temporal dynamics), financial time series and ecological variables; see Guadagnini and Neuman (2011), Leonardis et al. (2012) and references therein. In virtually all these examples ESS yields improved estimates of $\xi(q)$ and shows it to vary in a nonlinear fashion with q, a finding commonly taken to imply that the variables are multifractal. Yet computational analyses by

Guadagnini and Neuman (2011) have shown that this need not be the case: they found signals constructed from sub-Gaussian processes subordinated to truncated (additive, self-affine, monofractal) fractional Brownian motion (tfBm) to display ESS scaling as well as typical symptoms of multifractality, such as nonlinear scaling and intermittency, even though the signals differ from multifractals in a fundamental way (Neuman, 2010a, 2010b, 2011; Guadagnini et al., 2012).

Siena et al. (2012) have pointed out that since multifractals and fractional Laplace motions do not capture observed breakdowns in power-law scaling at small and large lags, they cannot explain how and why ESS does so. Instead, they have proven theoretically that ESS of data having a normal frequency distribution is theoretically consistent with tfBm. This allowed them to identify the functional form and estimate all parameters of the particular tfBm corresponding to log air permeability data collected by Tidwell and Wilson (1999) on the faces of a laboratory-scale block of Topopah Spring tuff. In this paper we employ ESS to analyze the scaling behaviors of two log permeability data sets showing heavy-tailed frequency distributions in three and two spatial dimensions, respectively. One set consists of 1-m scale pneumatic packer test data from six vertical and inclined boreholes spanning a decameters-scale block of unsaturated fractured tuffs near Superior, Arizona (Guzman et al., 1996). Another set contains pneumatic minipermeameter data measured at a spacing of 15 cm along three horizontal transects on a 21 m long and 6 m high outcrop of the Upper Cretaceous Straight Cliffs Formation, including lower-shoreface bioturbated and cross-bedded sandstone near Escalante, Utah (Castle et al., 2004). Our analysis (a) demonstrates that the two data sets are statistically and theoretically consistent with sub-Gaussian random fields subordinated to tfBm or truncated fractional Gaussian noise (tfGn) and (b) provides maximum likelihood estimates of parameters characterizing the corresponding Lévy stable subordinators and tfBm or tfGn functions.

THEORETICAL BACKGROUND

We start by recounting the theory that underlies our analysis of the data.

Sub-Gaussian processes subordinated to truncated fractional Brownian motion (tfBm)

Following Guadagnini et al. (2012) we limit (for simplicity) our theoretical exposé to a single space or time coordinate *x*, considering random functions $Y(x)$ characterized by constant mean and sub-Gaussian fluctuations (Samorodnitsky and Taqqu, 1994; Adler et al., 2010)

$$Y'(x;\lambda_l,\lambda_u)=W^{1/2}G'(x;\lambda_l,\lambda_u) \qquad (4)$$

about the mean. Here $W^{1/2}$ is an $\alpha/2-$stable random variable, totally skewed to the right of zero with width parameter $\sigma_W=\left(\cos\frac{\pi\alpha}{4}\right)^{2/\alpha}$, unit skewness $\beta=1$ and zero shift, $\mu=0$; for a precise definition of these parameters see (18) below. The variable *W* is independent of $G'(x;\lambda_l,\lambda_u)$, which in turn is a zero-mean Gaussian random field (or process) described by truncated power variogram (TPV)

$$\gamma_i^2(s;\lambda_l,\lambda_u)=\gamma_i^2(s;\lambda_u)-\gamma_i^2(s;\lambda_l) \qquad (5)$$

where, for $m=l,u$,

$$\gamma_i^2(s;\lambda_m)=\sigma^2(\lambda_m)\rho_i(s/\lambda_m)$$

$$\sigma^2(\lambda_m)=A\lambda_m^{2H}/2H$$

$$\rho_1(s/\lambda_m)=\left[1-\exp(-s/\lambda_m)+(s/\lambda_m)^{2H}\,\Gamma(1-2H,s/\lambda_m)\right] \qquad 0<H<0.5$$

$$\rho_2(s/\lambda_m)=\left[1-\exp\left(-\pi(s/\lambda_m)^2/4\right)+\left(\pi(s/\lambda_m)^2/4\right)^H\Gamma\left(1-H,\pi(s/\lambda_m)^2/4\right)\right] \qquad 0<H<1$$

A being a constant and $\Gamma(\cdot,\cdot)$ the incomplete gamma function (other functional forms of ρ being theoretically possible). For $\lambda_u<\infty$, the increments $\Delta Y'(x,s;\lambda_l,\lambda_u)$ are stationary with zero-mean symmetric Lévy stable distribution characterized by $1<\alpha\le 2$ and scale or width function (semi-structure function when $\alpha=2$; Samorodnitsky and Taqqu, 1994)

$$\sigma^\alpha(s;\lambda_l,\lambda_u)=\left[\gamma_i^2(s;\lambda_l,\lambda_u)\right]^{\alpha/2}. \qquad (6)$$

In the limits $\lambda_l \to 0$ and $\lambda_u \to \infty$ the TPV $\gamma_i^2(s;\lambda_l,\lambda_u)$ converges to a power variogram (PV) $\gamma_i^2(s) = A_i s^{2H}$ where $A_1 = A\Gamma(1-2H)/2H$ and $A_2 = A(\pi/4)^{2H/2}\Gamma(1-2H/2)/2H$. Correspondingly, $\sigma^\alpha(s;\lambda_l,\lambda_u)$ converges to a power law $\gamma_i^\alpha(s) = A_i s^{\alpha H}$ where $A_1 = A\Gamma(1-\alpha H)/\alpha H$ and $A_2 = A(\pi/4)^{\alpha H/2}\Gamma(1-\alpha H/2)/\alpha H$. The resultant nonstationary field $G'(x;0,\infty)$ thus constitutes fractional Brownian motion (fBm), its stationary increments $\Delta G'(x,s;0,\infty)$ forming fractional Gaussian noise (fGn); the nonstationary field $Y'(x;0,\infty)$ constructed from increments $\Delta Y'(s;0,\infty) = W^{1/2}\Delta G(x,s;0,\infty)$ constitutes fractional Lévy motion (fLm; fBm when $\alpha = 2$), the increments forming sub-Gaussian fractional Lévy noise (fLn or fsn for fractional stable noise, e.g. Samorodnitsky and Taqqu, 1994; Samorodnitsky, 2006).

It is possible to select a subordinator $W^{1/2} \geq 0$ having a heavy-tailed distribution other than Lévy such as, for example, a log-normal $W^{1/2} = e^V$ with $\langle V \rangle = 0$ and $\langle V^2 \rangle = (2-\alpha)^2$. Samples generated through subordination of truncated monofractal fBm in the above manner exhibit apparent multifractal scaling (Guadagnini et al., 2012).

Extended power-law scaling of sub-Gaussian processes subordinated to tfBm

It is important to note that whereas power-law scaling (2) implies ESS scaling (3), the reverse is not necessarily true because (3) follows from the more general relationship

$$S^q(s) \propto f(s)^{\xi(q)} \tag{7}$$

where $f(s)$ is a (possibly nonlinear) function of s (Kozubowski and Molz, 2011; Siena et al., 2012).

Following Neuman et al. (2012) we first consider subordinators $W^{1/2} \geq 0$ that have finite moments $\langle W^{q/2} \rangle$ of all orders q, such as the log-normal form mentioned earlier. Then, in a manner analogous to Siena et al. (2012), the central q^{th}-order moments of absolute values of zero-mean stationary increments $\Delta Y'(x,s;\lambda_l,\lambda_u)=W^{1/2}\Delta G'(x,s;\lambda_l,\lambda_u)$ can be expressed as

$$\begin{aligned} S^q &= \left\langle \left|\Delta Y'(s;\lambda_l,\lambda_u)\right|^q \right\rangle = \left\langle W^{q/2}\right\rangle \left\langle \left|\Delta G'(s;\lambda_l,\lambda_u)\right|^q\right\rangle \\ &= \left\langle W^{q/2}\right\rangle \left[\sqrt{2\gamma_i^2(s;\lambda_l,\lambda_u)}\right]^q (q-1)!! \begin{cases} \sqrt{\dfrac{2}{\pi}} & \text{if } q \text{ is odd} \\ 1 & \text{if } q \text{ is even} \end{cases} \end{aligned} \qquad q=1,2,3... \qquad (8)$$

Here !! represents double factorial, i.e., $q!! = q\,(q\text{-}2)\,(q\text{-}4)\ldots2$ if q is even and $q!! = q\,(q\text{-}2)\,(q\text{-}4)\ldots3$ if q is odd, and $\gamma_i^2(s;\lambda_l,\lambda_u)$ is the (truncated power) variogram (TPV) of $G'(x;\lambda_l,\lambda_u)$. The ratio between structure functions of order (q+1) and q is then

$$\frac{S^{q+1}}{S^q} = g(q) \begin{cases} \sqrt{\pi}\dfrac{q!!}{(q-1)!!}\sqrt{\gamma_i^2(s;\lambda_l,\lambda_u)} & \text{if } q \text{ is odd} \\ \dfrac{2}{\sqrt{\pi}}\dfrac{q!!}{(q-1)!!}\sqrt{\gamma_i^2(s;\lambda_l,\lambda_u)} & \text{if } q \text{ is even} \end{cases} \qquad q=1,2,3... \qquad (9)$$

where $g(q)$ depends on the choice of subordinator but not on s. In the log-normal case where $W^{1/2}=e^V$ with $\langle V\rangle=0$ and $\langle V^2\rangle=(2-\alpha)^2$ one obtains $\langle W^{q/2}\rangle=\exp\left[q^2(2-\alpha)^2/2\right]$ and $g(q)=\langle W^{(q+1)/2}\rangle/\langle W^{q/2}\rangle=\exp\left[(1+2q)(2-\alpha)^2/2\right]$. It then follows from (8) and (9) that

$$S^{q+1} = g(q) \begin{cases} \sqrt{\dfrac{\pi}{2}}\left[\sqrt{\dfrac{\pi}{2}}\dfrac{1}{(q-1)!!}\right]^{\frac{1}{q}}\dfrac{q!!}{(q-1)!!}\left[S^q\right]^{1+\frac{1}{q}} & \text{if } q \text{ is odd} \\ \sqrt{\dfrac{2}{\pi}}\left[\dfrac{1}{(q-1)!!}\right]^{\frac{1}{q}}\dfrac{q!!}{(q-1)!!}\left[S^q\right]^{1+\frac{1}{q}} & \text{if } q \text{ is even} \end{cases} \qquad q=1,2,3... \qquad (10)$$

showing that log S^{q+1} is linear in log S^q, in accord with the ESS expression (3), regardless of the choice of subordinator or the model employed for $\left\langle \Delta G'(s;\lambda_l,\lambda_u)^2\right\rangle$. On log-log plot, this line is characterized by a slope which tends to unity as $q \to \infty$, being equal to 2 at q = 1. Equation (10) is a consequence of the equivalence between (8) and ESS expression (7) in which now $f(s)=\left[\sqrt{2\gamma^2(s;\lambda_l,\lambda_u)}\right]$. It shows that extended power-law scaling, or ESS, at all lags is an intrinsic property of sub-Gaussian processes subordinated to tfBm (or tfGn) with subordinators, such as the log normal, which have finite moments of all orders.

We noted earlier that, in the limits $\lambda_l \to 0$ and $\lambda_u \to \infty$, the TPV $\gamma_i^2(s;\lambda_l,\lambda_u)$ converges to a PV $\gamma_i^2(s)=A_i s^{2H}$. It follows that (8) can be rewritten in terms of a power-law

$$S^q=\left\langle W^{q/2}\right\rangle (q-1)!!\left[\sqrt{2A_i}\right]^q s^{qH}\begin{cases}\sqrt{\dfrac{2}{\pi}} & if\ q\ is\ odd\\ 1 & if\ q\ is\ even\end{cases} \qquad q=1,2,3... \qquad (11)$$

where it is clear that a log-log plot of S^q versus s is linear at all lags and associated with a constant slope qH.

Following Neuman et al. (2012) we now consider subordinators $W^{1/2}\geq 0$ that have divergent ensemble moments $\left\langle W^{q/2}\right\rangle$ of all orders $q\geq 2\alpha$, as does the previously discussed Lévy subordinator with stability index α. In practical applications, $\left\langle\left|\Delta Y'(s;\lambda_l,\lambda_u)\right|^q\right\rangle$ is typically estimated through a sample structure function

$$S^q_{|\Delta Y|,N,M}(s;\lambda_l,\lambda_u)=\frac{1}{N(s)M}\sum_{m=1}^{M}\sum_{n=1}^{N(s)}\left|\Delta y_m(x_n,s;\lambda_l,\lambda_u)\right|^q \qquad q=1,2,3... \qquad (12)$$

where $\Delta y_m(x_n,s;\lambda_l,\lambda_u)$ denotes a collection of $M<\infty$ sets of $N(s)<\infty$ sampled increments each; for simplicity, we ignore possible variations of $N(s)$ and x_n with m. Writing $\Delta y_m(x_n,s;\lambda_l,\lambda_u)=w_m^{1/2}\Delta g_m(x_n,s;\lambda_l,\lambda_u)$ where $\Delta g_m(x_n,s;\lambda_l,\lambda_u)$ represents samples of $\Delta G'(s;\lambda_l,\lambda_u)$ allows rewriting (12) as

$$S^{q}_{|\Delta Y|,N,M}\left(s;\lambda_l,\lambda_u\right)=\frac{1}{M}\sum_{m=1}^{M}w_m^{q/2}\,\frac{1}{N\left(s\right)}\sum_{n=1}^{N(s)}\left|\Delta g_m\left(x_n,s;\lambda_l,\lambda_u\right)\right|^{q}. \qquad q=1,2,3... \qquad (13)$$

Since order $q\geq 2\alpha$ moments of $w_m^{1/2}$ diverge while all moments of $\Delta g_m\left(x_n,s;\lambda_l,\lambda_u\right)$ converge, one can approximate (13) for a sufficiently large sample size $N\left(s\right)$ by

$$\begin{aligned}S^{q}_{|\Delta Y|,N,M}\left(s;\lambda_l,\lambda_u\right)&\simeq\left(\frac{1}{M}\sum_{m=1}^{M}w_m^{q/2}\right)\left\langle\left|\Delta G'\left(s;\lambda_l,\lambda_u\right)\right|^{q}\right\rangle\\&=\left(\frac{1}{M}\sum_{m=1}^{M}w_m^{q/2}\right)\left[\sqrt{2\gamma_i^2\left(s;\lambda_l,\lambda_u\right)}\right]^{q}\left(q-1\right)!!\begin{cases}\sqrt{\dfrac{2}{\pi}} & if\ q\ is\ odd\\ 1 & if\ q\ is\ even\end{cases}\end{aligned} \qquad q=1,2,3... \qquad (14)$$

which, for finite *M*, is always finite. One can then write

$$\frac{S^{q+1}_{|\Delta Y|,N,M}\left(s;\lambda_l,\lambda_u\right)}{S^{q}_{|\Delta Y|,N,M}\left(s;\lambda_l,\lambda_u\right)}\simeq\frac{\sum_{m=1}^{M}w_m^{(q+1)/2}}{\sum_{m=1}^{M}w_m^{q/2}}\begin{cases}\sqrt{\pi}\dfrac{q!!}{\left(q-1\right)!!}\sqrt{\gamma_i^2\left(s;\lambda_l,\lambda_u\right)} & if\ q\ is\ odd\\ \dfrac{2}{\sqrt{\pi}}\dfrac{q!!}{\left(q-1\right)!!}\sqrt{\gamma_i^2\left(s;\lambda_l,\lambda_u\right)} & if\ q\ is\ even\end{cases} \qquad q=1,2,3... \qquad (15)$$

or, in analogy to (10),

$$S^{q+1}_{|\Delta Y|,N,M}\left(s;\lambda_l,\lambda_u\right)\simeq\frac{\sum_{m=1}^{M}w_m^{(q+1)/2}}{\sum_{m=1}^{M}w_m^{q/2}}\begin{cases}\sqrt{\dfrac{\pi}{2}}\left[\sqrt{\dfrac{\pi}{2}}\dfrac{1}{\left(q-1\right)!!}\right]^{\frac{1}{q}}\dfrac{q!!}{\left(q-1\right)!!}\left[S^{q}_{|\Delta Y|,N,M}\left(s;\lambda_l,\lambda_u\right)\right]^{1+\frac{1}{q}} & if\ q\ is\ odd\\ \sqrt{\dfrac{2}{\pi}}\left[\dfrac{1}{\left(q-1\right)!!}\right]^{\frac{1}{q}}\dfrac{q!!}{\left(q-1\right)!!}\left[S^{q}_{|\Delta Y|,N,M}\left(s;\lambda_l,\lambda_u\right)\right]^{1+\frac{1}{q}} & if\ q\ is\ even\end{cases}$$

$$q=1,2,3... \qquad (16)$$

This indicates that $S^{q+1}_{|\Delta Y|,N,M}\left(s;\lambda_l,\lambda_u\right)$ is approximately linear in $S^{q}_{|\Delta Y|,N,M}\left(s;\lambda_l,\lambda_u\right)$ on log-log scale, in accord with ESS expression (3), regardless of the functional form $\left\langle\Delta G'\left(s;\lambda_l,\lambda_u\right)^2\right\rangle$ takes. The slope of this line is characterized by the same asymptotic behavior as that observed before. The approximate equivalence between (14) and the ESS expression (7), where $f\left(s\right)=\left[\sqrt{2\gamma_i^2\left(s;\lambda_l,\lambda_u\right)}\right]$, is the basis for

(16) and its asymptotic tendency. It follows that extended power-law scaling, or ESS, at all lags is an intrinsic property of samples from sub-Gaussian processes subordinated to tfBm (or tfGn) with subordinators, such as Lévy, which have divergent ensemble moments of orders $q \geq 2\alpha$.

Note that in the limits $\lambda_l \to 0$ and $\lambda_u \to \infty$, (14) becomes a power-law

$$S^q \simeq \left(\frac{1}{M} \sum_{m=1}^{M} w_m^{q/2} \right) (q-1)!! \left[\sqrt{2A_i} \right]^q s^{qH} \begin{cases} \sqrt{\dfrac{2}{\pi}} & \text{if } q \text{ is odd} \\ 1 & \text{if } q \text{ is even} \end{cases} \qquad q = 1,2,3... \tag{17}$$

rendering log S^q linear in log s with constant slope qH.

ANALYSIS OF LOG AIR PERMEABILITIES FROM BOREHOLE TESTS IN UNSATURATED FRACTURED TUFF NEAR SUPERIOR, ARIZONA

We analyze (natural) log air permeability (Y = log k, k being permeability) data from unsaturated fractured tuff at a former University of Arizona research site near Superior, Arizona. Our analysis focuses on log k values obtained by Guzman et al. (1996) from steady state interpretations of 184 pneumatic injection tests in 1-m long intervals along 6 boreholes at the site (Fig. 1). Five of the boreholes (V2, W2a, X2, Y2, Z2) are 30 m long and one (Y3) has a length of 45 m; five (W2a, X2, Y2, Y3, Z2) are inclined at 45^{o} and one (V2) is vertical. The boreholes cover a horizontal area of 25.83 × 21.43 m^2.

Riva et al. (2012) hypothesized that the data derive from a Lévy stable distribution, estimated the parameters of this distribution by three different methods and examined the degree to which each distribution estimate fits the data. We focus here on parameter estimates obtained by them using a maximum likelihood (ML) approach applied to a log characteristic function

$$\ln \left\langle e^{i\phi X} \right\rangle = i\mu\phi - \sigma^\alpha |\phi|^\alpha \left[1 + i\beta \operatorname{sign}(\phi) \omega(\phi,\alpha) \right] \qquad \omega(\phi,\alpha) = \begin{cases} -\tan \dfrac{\pi\alpha}{2} & \text{if } \alpha \neq 1 \\ \dfrac{2}{\pi} \ln|\phi| & \text{if } \alpha = 1 \end{cases} \tag{18}$$

of an α-stable variable, X; ϕ is a real-valued parameter; $\text{sign}(\phi)$ = 1, 0, −1 if ϕ > 0, = 0, < 0, respectively; $\alpha \in$ (0, 2] is stability or Lévy index; $\beta \in$ [-1, 1] is skewness parameter; σ > 0 is scale or width parameter; and μ is shift or location parameter. The authors found $Y' = \log k - \langle \log k \rangle$ to fit (18) with parameter estimates $\hat{\alpha} = 2.0 \pm 0.00$, $\hat{\sigma} = 1.42 \pm 0.15$ and $\hat{\mu} = 0.00 \pm 0.29$. Note that it is difficult to estimate β reliably when $\hat{\alpha} \approx 2$ because, at $\alpha = 2$, the distribution is insensitive to β.

Figure 2a compares the frequency distribution of the data with their ML estimated probability density function and Fig. 2b depicts a corresponding Q-Q plot. The fits are ambiguous enough to suggest that their near-Gaussian appearance could in fact indicate a Lévy stable distribution with α just slightly smaller than 2. That this is likely the case follows from the tendency of $\hat{\alpha}$, fitted to the distributions of log k increments, to increase from 1.46±0.21 at 1 m lag through 1.84±0.16 at lag 2 m and 1.91±0.12 at lag 3 m to 2 at lags equal to or exceeding 4 m. Increments corresponding to lags smaller than 4 m are thus clearly heavy tailed (and hence non-Gaussian) as evidenced further by Fig. 3, which compares frequency distributions and ML estimated probability density functions of $Y' = \log k - \langle \log k \rangle$ data and log k increments at lags 1 m, 2 m and 5 m. Had the original log k data been genuinely Gaussian, the same would have to be true for their increments.

Figure 4 depicts omnidirectional structure functions, S_N^q, of orders q = 1, 2, 3, 4, 5 computed for the same data according to (12). To compute them we ascribe each measurement to the midpoint of the corresponding 1-m scale borehole test interval. We then associate (as is common in geostatistical practice) data pairs separated by distances of 1.5 – 2.5 m with a lag of 1 m, those separated by distances of 2.5 – 3.5 m with a lag of 2 m, and so on up to the largest separation distances of 29.5 – 30.5 m, which we associate with a lag of 30 m. Figure 5 shows that the number of data pairs associated in this manner with each lag is largest at intermediate lags, causing log k increments to be comparatively undersampled at small and large lags. Such undersampling may explain in part why the structure functions in Fig. 4 scale differently with separation scale at small, intermediate and large lags. Standard moment analysis would entail fitting straight lines to these functions at intermediate lags by regression and considering their slopes to represent power-law exponents $\xi(q)$ in (2). However, deciding what constitutes an appropriate range of intermediate lags for such analysis would, in the case of Fig. 4, be fraught with ambiguity.

We avoid this ambiguity by plotting in Fig. 6 S_N^q versus S_N^{q-1} for $2 \le q \le 5$ on log-log scale for the entire range of available lags. Also shown in Fig. 6 are linear regression fits to each of these relationships, the corresponding regression equations and coefficients of determination, R^2. As the latter exceed 0.99 in all cases, we conclude with a high degree of confidence that S_N^q is a power $\beta(q,q-1)$ of S_N^{q-1} for $2 \le q \le 5$ at all lags, in accord with ESS expression (3). This power, given by the slopes of the regression lines in Fig. 6, decreases from 1.66 at $q = 2$ through 1.29 at $q = 3$ and 1.17 at $q = 4$ to 1.12 to $q = 5$, appearing to tend asymptotically toward 1 with increasing q. Considering S_N^q to vary as a power $\xi(q)$ of s according to (2) at intermediate lags, as suggested by Fig. 4, allows expressing the power of S_N^q in (3) as $\beta(q,q-1) = \xi(q)/\xi(q-1)$. Asymptotic tendency of $\beta(q,q-1)$ toward 1 then implies asymptotic tendency of $\xi(q)$ toward a straight line. This commonly observed tendency, which the multifractal literature attributes to divergence of higher-order moments, is according to our theory (Neuman, 2010a; Guadagnini and Neuman, 2011) unrelated to such divergence, arising instead from the presence of an upper cutoff scale, λ_u.

Figure 4 includes two vertical broken lines demarcating a midrange of lags within which $\log S_N^1$ appears to be quite unambiguously linear in $\log s$. Fitting a straight line to the corresponding data by regression yields $\xi(1) = 0.56$ with a high coefficient of determination, $R^2 = 0.97$. This, together with values of $\beta(q, q-1) = \xi(q) / \xi(q-1)$ corresponding to $2 \leq q \leq 5$ in Fig. 6, allows us to compute $\xi(q)$ for this entire range of q values, as depicted in Fig. 7. Figure 7 also includes for reference one straight line having slope $\xi(1) = 0.56$ and another having slope $H = 0.33$, estimated for the same data by Riva et al. (2012). Their estimate follows from a treatment of the data as a sample from a sub-Gaussian random field subordinated to tfBm via a Lévy stable subordinator. It is evident that $\xi(q)$ in Fig. 7 is nonlinear concave in q in the range $2 \leq q \leq 5$. Though such nonlinear scaling is typical of multifractals or fractional Laplace motions, we have demonstrated theoretically earlier that it is in fact consistent with a random field subordinated to tfBm via a heavy-tailed subordinator.

ANALYSIS OF NITROGEN MINIPERMEAMETER DATA FROM SANDSTONE NEAR ESCALANTE, UTAH

Castle et al. (2004) describe nitrogen minipermeameter measurements conducted on a flat, nearly vertical outcrop of Straight Cliffs Formation sandstones about 10 km northwest of Escalante, Utah. The outcrop, measuring approximately 21 m across and 6 m high, includes a lower bioturbated facies and an upper cross-bedded facies (Fig. 8). A total of 515 permeability measurements were taken in triplicate at a sample spacing of 15 cm along three horizontal transects (380 measurements) and four vertical profiles (135 measurements). Castle et al. (2004) found that whereas sample statistics of (natural) log permeability, log k, vary depending on which facies are considered, the frequency distributions of horizontal log k increments in the two facies are similar. Lu et al. (2002) used a fBm model to generate log k increments within a mix of distinct facies. They showed that, when data from different facies are analyzed jointly, the simulated log k increments exhibit an apparent non-Gaussian distribution. They concluded that observed Lévy-like behavior of sample probability distributions of permeability data can in some cases be an artifact of mixing data from disparate facies. Accordingly, Moltz et al. (2007) focused their analysis on increments along horizontal transects D and H (Fig. 8) within the lower bioturbated facies. They found the horizontal log k increments to be well represented by a fractional Laplace noise model. We note however that this same model would not have allowed them to characterize statistically the log k data themselves.

In this paper we analyze the frequency distributions and scaling of log k values and their horizontal increments (*a*) along transects D and H within the lower bioturbated facies and (b) jointly along transects D, H and X (Fig. 8) in the two facies. We also attempted to perform a similar analysis of log k values and their increments along the four vertical transects at the site but found the corresponding samples too small to yield meaningful statistics.

Transect H contains 133 data points, transect D 136 points and transect X 111 points. In a manner consistent with Riva et al. (2012), we analyze the frequency distribution of $Y' = \log k - \langle \log k \rangle$ and use the computer code STABLE (Nolan 1997, 2001) to obtain reliable ML estimates of stable densities. Fig. 9a compares the frequency distribution of Y' data from transects D and H on semi-logarithmic scale with a probability density function (pdf) fitted to it via ML. Treating the data as if they were Lévy stable yields ML parameter estimates $\hat{\alpha}$ = 1.99 ± 0.05, $\hat{\sigma}$ = 0.28 ± 0.02, β = 0 and $\hat{\mu}$ = 0.00 ± 0.05. As $\hat{\alpha} \approx 2$, the distribution appears to be Gaussian. Yet Kolmogorov – Smirnov and Shapiro – Wilk tests reject the Gaussianity hypothesis at a 0.1% significance level. The frequency distribution of Y' data from all three horizontal transects D, H and X in Fig. 9b is positively skewed with ML parameter estimates $\hat{\alpha}$ = 1.20 ± 0.12, $\hat{\beta}$ = 1, $\hat{\sigma}$ = 0.39 ± 0.04 and $\hat{\mu}$ = 0.726 ± 0.07. We conclude that the two facies contain distinctly different log permeability populations Y'.

Figure 10 compares frequency distributions and ML estimated probability density functions of log k increments along transects D and H, and jointly along transects D, H and X, at horizontal lags of

0.15 m, 0.45 m, 1.5 m and 4.5 m. Whereas at small lags the two distributions are similar (Figs. 10a, 10b), at larger lags the joint set from both facies exhibits heavier tails. Kolmogorov – Smirnov and Shapiro – Wilk tests generally reject the hypothesis that the increments, at any lag, are Gaussian at a 0.1% significance level. A χ^2 test applied to horizontal increments along transects D and H at a lag of 0.15 m by Castle et al. (2004) has shown them to be Gaussian only at a 51% confidence level.

As shown in Fig. 11, ML estimates $\hat{\alpha}$ of the Lévy index of log permeability increments along transects D and H vary from 1.89 ± 0.13 at horizontal lag 0.15 m through 1.86 ± 0.14 at lag 0.3 m, 1.66 ± 0.18 at lag 0.45 m, 1.86 ± 0.14 at lag 0.6 m, 1.82 ± 0.16 at lag 0.75 m, 1.99 at lag 0.9 m to 2.00 at larger lags. Hence the distributions of the increments have heavier tails at small than at larger lags. ML estimates $\hat{\alpha}$ obtained from all three horizontal transects oscillate around 1.75 without any identifiable trend. ML estimates $\hat{\sigma}$ of the scale parameter in Fig. 11 increase monotonically with lag toward a constant asymptote of 0.32 for data along transects D and H and 0.44 for data along transects D, H and X. Both phenomena are consistent with the observation of Lu et al (2002) that mixing data from the two facies may cause the tails of incremental frequency distributions to increase.

Results based on data sampled along transects D and H in the bioturbated sandstone facies are consistent with a sub-Gaussian random field subordinated to tfBm via a Lévy stable subordinator. The observed increase in $\hat{\alpha}$ with lag is consistent with a version of such a field considered by Riva et al. (2012). Following their approach, (6) allows us to estimate the associated Hurst coefficient from the log-log slope of $\hat{\sigma}(s)$ in Fig. 11 at lags small enough to avoid the asymptote. This slope yields an estimate $H = 0.13$. From (6) it follows that, asymptotically, $\hat{\sigma}_G^2 = 2\hat{\sigma}^2$ where $G'\left(s;\lambda_l,\lambda_u\right)$ is our tfBm. This, coupled with our ML estimates of $\hat{\sigma}$ for the $\log k - \left\langle \log k \right\rangle$ data, yields $\hat{\sigma}_G^2 = 2\times(0.28)^2 = 0.16$. Having thus estimated H and σ_G^2 we are now in a position to estimate the remaining parameters of the

TPV $\gamma_G^2\left(s;\lambda_l,\lambda_u\right)$ of $G'\left(s;\lambda_l,\lambda_u\right)$ defined in (5). Setting $i=1$ in (5) we obtain the following ML estimates of the cutoff scales, $\lambda_l \approx 0.0$ m and $\lambda_u = 16.97$ m (with 95% confidence limits 3.45 m and 30.47 m; setting $i = 2$ yields a less satisfactory fit, suggesting that $i = 1$ is a better choice). Our estimate of λ_l is consistent with the small support scale of the minipermeameter. Our estimate of λ_u is slightly smaller than the lengths of the D and H transects (on the order of 20 m), as expected from theory (Guadagnini et al., 2012). Figure 12 depicts experimental scale parameters and their theoretical equivalents based on the above ML estimates of $\hat{\sigma}_G^2$, H, λ_l and λ_u. Dashed curves in the figure represent 95% confidence limits of corresponding λ_u estimates.

Results based on data sampled jointly along transects D, H and X in the bioturbated and cross-bedded sandstone facies are not fully consistent with our theory, which considers both Y' and its increments to have symmetric distributions. As the distributions of the corresponding increments are in fact symmetric, it is possible to treat these increments as random field subordinated to truncated fractional Gaussian noise (tfGn) forming truncated sub-Gaussian fractional Lévy noise (tfLn) as discussed by Riva et al. (2012). Such processes are characterized by Lévy indices α that are independent of lag. Repeating the above procedure we obtain estimates $H = 0.21$, $\hat{\sigma}_G^2 \approx 0.34$, $\lambda_l \approx 0.0$ m and $\lambda_u = 29.04$ m (with 95% confidence limits 16.23 m and 41.85 m). Though this estimate of H exceeds that obtained previously on the basis of data from transects D and H alone, both are small and indicative of strong anti-persistence typical of log permeabilities in fractured and porous rocks worldwide (Neuman, 1990).

Figure 13 depicts sample structure functions of order q = 1, 2, 3, 4, 5, 6 for the data collected along transects D and H. Vertical lines demarcate the midrange of lags within which a regression line, the slope of which was taken to represent $\xi(1)$, had been fitted to S_N^1. The latter was found to be $\xi(1)$ = 0.12 with coefficient of determination $R^2 = 0.93$. This value is only slightly smaller than that obtained earlier from the log-log slope of $\hat{\sigma}(s)$ in Fig. 11. Figure 14 shows log-log plots of S_N^q versus S_N^{q-1} for 2 $\leq q \leq$ 6 and corresponding linear regression fits. The fits are characterized by coefficients of determination, R^2, two of which exceed 0.98 and three 0.99. The slope of the fitted lines decreases from 1.86 at q = 2 through 1.40 at q = 3, 1.25 at q = 4, and 1.19 at q = 5 to 1.15 at q = 6, appearing to tend asymptotically toward 1 as expected. Adopting the above value of $\xi(1)$ = 0.12 allows computing $\xi(q)$ for $2 \leq q \leq 6$ using the ESS relationship $\beta(q, q-1) = \xi(q) / \xi(q-1)$. The results are plotted in Fig. 15 together with straight lines having slopes $\xi(1) = 0.12$ and $H = 0.13$. It is clear that $\xi(q)$ is nonlinear concave in q within the range $2 \leq q \leq 6$. Though such nonlinear scaling is typical of multifractals or fractional Laplace motions, we have demonstrated theoretically earlier that it is in fact consistent with a random field subordinated to tfBm via a heavy-tailed subordinator.

Qualitatively similar results (details not given) are obtained from structure functions of order q computed jointly for horizontal increments along transects D, H and X in the two facies. Following the above procedure we obtain $\xi(1)$ = 0.26, consistent with an analysis of $\hat{\sigma}(s)$ which yields H = 0.21. Applying ESS yields a nonlinear concave functional form for $\xi(q)$ in Fig. 16, which also depicts for reference straight lines having slopes $\xi(1) = 0.26$ and $H = 0.21$.

CONCLUSIONS

Our analyses lead to the following major conclusions:

1. Extended power-law scaling, commonly known as extended self similarity or ESS, is an intrinsic property of sub-Gaussian random fields or processes subordinated to truncated fractional Brownian motion (tfBm) or truncated fractional Gaussian noise (tfGn). Such fields and processes are theoretically consistent with standard power-law scaling at intermediate lags and with ESS at all lags, including small and large lags at which power-law scaling breaks down.

2. Multifractals and fractional Laplace motions are theoretically consistent with standard power-law scaling at all lags. As such, they neither reproduce observed breakdown in power-law scaling at small and large lags nor explain how ESS extends power-law scaling to such lags.

3. 1-m scale pneumatic packer test data from unsaturated fractured tuffs near Superior, Arizona, and nitrogen minipermeameter data from bioturbated and cross-bedded sandstones near Escalante, Utah, and their increments, show heavy-tailed frequency distributions that can be fitted with a high level of confidence to Lévy stable distributions.

4. Order q sample structure functions of each data set scale as a power $\xi(q)$ of separation scale or lag, s, over limited ranges of s. ESS extends this range to all lags and yields a nonlinear concave functional relationship between $\xi(q)$ and q.

5. The data sets we analyze are consistent with sub-Gaussian random fields subordinated to tfBm or to tfGn via Lévy stable subordinators.

6. This consistency allows estimating all tfBm or tfGn parameters (most notably the Hurst exponent and upper/lower cutoff scales) solely on the basis of the corresponding truncated power variograms.

7. The consistency further implies that nonlinear scaling of both data sets, manifested in a nonlinear concave relationship between their power-law exponents $\xi(q)$ and q, is not an indication of multifractality but an artifact of sampling as explained theoretically by Neuman (2010a) and Guadagnini et al. (2012).

ACKNOWLEDGEMENTS

This work was supported in part through a contract between the University of Arizona and Vanderbilt University under the Consortium for Risk Evaluation with Stakeholder Participation (CRESP) III, funded by the U.S. Department of Energy. Funding from the Politecnico di Milano

(GEMINO, Progetti di ricerca 5 per mille junior) is also acknowledged. We are grateful to Fred Molz for sharing with us the experimental Utah database.

REFERENCES

Adler, R.J., Samorodnitsky G., and Taylor J.: Excursion sets of stable random fields, Adv. Appl. Probab., 42, 293-318, 2010.

Benzi, R., Ciliberto, S., Baudet, C., Chavarria, G. R., and Tripiccione, R.: Extended self-similarity in the dissipation range of fully developed turbulence, Europhys. Lett., 24, 275-279, doi:10.1209/0295-5075/24/4/007, 1993a.

Benzi, R., Ciliberto, S., Tripiccione, R., Baudet, C., Massaioli, F., and Succi, S.: Extended self-similarity in turbulent flows, Phys. Rev. E, 48, R29–R32, doi:10.1103/PhysRevE.48.R29, 1993b.

Castle, J. W., Molz F J., Lu S., and Dinwiddie C.L.: Sedimentology and fractal-based analysis of permeability data, John Henry Member, Straight Cliffs Formation (Upper Cretaceous), Utah, USA, J. Sed. Res., 74, 2, 270-284, 2004.

Chakraborty, S., Frisch U., and Ray S. S.: Extended self-similarity works for the Burgers equation and why, J. Fluid Mech., 649, 275-285, doi:10.1017/S0022112010000595, 2010.

Ganti, V., Singh, A., Passalacqua, P., and Foufoula-Georgiu, E.: Subordinated Brownian motion model for sediment transport, Phys. Rev. E, 80, 011111, doi:1539-5663755/2009/80(1)/011111(8), 2009.

Guadagnini, A. and Neuman S. P.: Extended Self-Affinity of Signals Exhibiting Apparent Multifractality, Geophys. Res. Lett., 38, L13403, doi:10.1029/2011GL047727, 2011.

Guadagnini, A., Neuman, S. P., and Riva, M.: Numerical Investigation of Apparent Multifractality of Samples from Processes Subordinated to Truncated fBm, Hydrol. Process., doi:10.1002/hyp.8358, published on line, 2012.

Guzman, A. G., Geddis A. M., Henrich M. J., Lohrstorfer C. F., and Neuman S. P.: Summary of Air Permeability Data From Single-Hole Injection Tests in Unsaturated Fractured Tuffs at the Apache Leap Research Site: Results of Steady-State Test Interpretation. NUREG/CR-6360, U.S. Nuclear Regulatory Commission, Washington, D.C., 1996.

Kozubowski, T. J. and Molz, F. J.: Interactive discussion of the discussion paper "Extended power-law scaling of air permeabilities measured on a block of tu?" by Siena, M., Guadagnini, A., Riva, M., and Neuman, S. P., Hydrol. Earth Syst. Sci. Discuss., 8, 7805-7843, 2011, doi:10.5194/hessd-8-7805-2011, 2011.

Kozubowski, T. J., Meerschaert, M. M., and Podgorski, K.: Fractional Laplace motion, Adv. Appl. Probab., 38, 451-464, doi:10.1239/aap/1151337079, 2006.

Leonardis, E., Chapman S. C., and Foullon C.: Turbulent characteristics in the intensity fluctuations of a solar quiescent prominence observed by the Hinode Solar Optical Telescope, The Astrophysical Journal, 745, 185 (8pp), doi:10.1088/0004-637X/745/2/185, 2012.

Lu, S., Molz F. J., Fogg G. E., and Castle J. W.: Combining stochastic facies and fractal models for representing natural heterogeneity, Hydrogeol. J., 10, 475-482, 2002.

Meerschaert, M. M., Kozubowski, T. J., Molz, F. J., and Lu, S.: Fractional Laplace model for hydraulic conductivity, Geophys. Res. Lett., 31, L08501, doi:10.1029/2003GL019320, 2004.

Molz, F. J., Kozubowski, T. J., Podgórski K., and Castle, J. W.: A generalization of the fractal/facies model, Hydrogeol. J., 15, 4, 809-816, doi:10.1007/s10040-006-0154-9, 2007.

Neuman, S. P.: Universal Scaling of Hydraulic Conductivities and Dispersivities in Geologic Media, Water Resour. Res., 26, 8, 1749-1758, 1990.

Neuman, S. P.: Apparent/spurious multifractality of data sampled from fractional Brownian/Lévy motions, Hydrol. Process., 24, 2056-2067, doi:10.1002/hyp.7611, 2010a.

Neuman, S. P.: Apparent/spurious multifractality of absolute increments sampled from truncated fractional Gaussian/Lévy noise, Geophys. Res. Lett., 37, L09403, doi:10.1029/2010GL043314, 2010b.

Neuman, S. P.: Apparent multifractality and scale-dependent distribution of data sampled from self-affine processes, Hydrol. Process., 25, 1837–1840, doi:10.1002/hyp.7967, 2011.

Neuman, S. P., Guadagnini A., Riva M., and Siena M.: Recent Advances in Statistical and scaling analysis of earth and environmental variables, in Recent Advances in Hydrogeology, Cambridge University Press, Cambridge UK, (invited), under review, 2012.

Nolan, J.P.: Numerical computation of stable densities and distribution functions, Commun. Stat. Stoch. Models, 13(4), 759-774, 1997.

Nolan, J.P.: Maximum likelihood estimation of stable parameters, In: Barndorff-Nielsen O.E., Mikosch T., Resnick S.I. (Eds), Levy processes: theory and applications. Birkhäuser, Boston, 379-400, 2001.

Riva, M., Neuman S. P., and Guadagnini A.: Sub-Gaussian model of processes with heavy tailed distributions applied to permeabilities of fractured tuff, Stoch. Environ. Res. Risk Assess., doi:10.1007/s00477-012-0576-y, published on line, 2012.

Samorodnitsky, G.: Long memory and self-similar processes, Annales de la Faculte' des Sciences de Toulouse, 15, 107-123, 2006.

Samorodnitsky, G., and Taqqu M.: Stable Non-Gaussian Random Processes. New York: Chapman and Hall, 1994.

Siena, M., Guadagnini A., Riva M., and Neuman S. P.: Extended power-law scaling of air permeabilities measured on a block of tuff, Hydrol. Earth Syst. Sci., 16, 29-42, doi:10.5194/hess-16-29-2012, 2012

Stumpf, M. P. H., and Porter M. A.: Critical truths about power laws, Science, 335, 665-666, 2012.

Tidwell, V. C. and Wilson, J. L.: Upscaling experiments conducted on a block of volcanic tuff: results for a bimodal permeability distribution, Water Resour. Res., 35, 3375–3387, doi:10.1029/1999WR900161, 1999.

Figures Captions

Fig. 1. Spatial locations along each borehole of Arizona data. Modified after Guzman et al. (1996).

Fig. 2. (a) Frequency distribution (symbols) and ML estimated probability density function (solid curve) of Arizona data; (b) Q-Q plot of empirical data versus theoretical estimate of stable distribution.

Fig. 3. Frequency distributions (symbols) and ML estimated probability density functions (curves) of Arizona $Y' = \log k - \langle \log k \rangle$ data (red) and log k increments at lags s = 1 m (black), 2 m (green), and 5 m (blue).

Fig. 4. Sample structure functions of orders q = 1, 2, 3, 4, 5 of Arizona data versus lag. Light vertical broken lines demarcate midrange of lags within which heavy inclined broken line, with slope taken to represent $\xi(1)$, was fitted to S_N^1.

Fig. 5. Number of Arizona data pairs associated with each lag.

Fig. 6. Log-log variations of S_N^q of Arizona data with S_N^{q-1} for $2 \le q \le 5$. Solid lines represent indicated regression fits.

Fig. 7. $\xi(q)$ as a function of q (symbols) obtained via ESS based on $\xi(1) = 0.56$ computed for Arizona data by method of moments. Solid line has slope $\xi(1) = 0.56$ and dashed line slope H = 0.33 estimated for these data based on our theory, using maximum likelihood, by Riva et al. (2012).

Fig. 8. Locations of nitrogen minipermeameter measurements along sandstone outcrop near Escalante, Utah. Modified after Castle et al. (2004).

Fig. 9. Frequency distribution (symbols) and ML estimated probability density function (curves) of Utah $Y' = \log k - \langle \log k \rangle$ data on horizontal (a) transects D and H (bioturbated sandstone) and (b) transects D, H and X (bioturbated sandstone and cross-bedded sandstone).

Fig. 10. Frequency distributions (symbols) and ML estimated probability density functions (curves) of Utah log k increments for transects D and H (bioturbated sandstone) and transects D, H and X (bioturbated sandstone and cross-bedded sandstone) at horizontal lags (a) 0.15 m, (b) 0.45 m, (c) 1.5 m, and (d) 4.5 m.

Fig. 11. Variations of ML Lévy index estimates $\hat{\alpha}$ and scale parameter estimates $\hat{\sigma}$ of Utah log permeability increments with horizontal lag for transects D and H (bioturbated sandstone) and transects D, H and X (bioturbated sandstone and cross-bedded sandstone).

Fig. 12. Experimental scale parameter (diamonds) and their theoretical equivalents based on ML fit (solid curve) of TPV (6) based on data from transects D and H (bioturbated sandstone). Dashed curves represent 95% confidence limits of corresponding λ_u estimates.

Fig. 13. Sample structure functions of order q = 1, 2, 3, 4, 5, 6 of Utah data from transects D and H (bioturbated sandstone). Light vertical broken lines demarcate midrange of lags within which heavy inclined broken line, with slope taken to represent $\xi(1)$, was fitted to S_N^1.

Fig. 14. Log-log variations of S_N^q of Utah data from transects D and H (bioturbated sandstone) with S_N^{q-1} for $2 \leq q \leq 6$. Solid lines represent indicated regression fits. Linear regression equations and related regression coefficients (R^2) are also reported.

Fig. 15. $\xi(q)$ as a function of q (symbols) obtained via ESS based on $\xi(1) = 0.12$ computed for Utah data from transects D and H (bioturbated sandstone) by method of moments. Solid line has slope $\xi(1) = 0.12$ and broken line has slope $H = 0.13$.

Fig. 16. $\xi(q)$ as a function of q (symbols) obtained via ESS based on $\xi(1) = 0.26$ computed for Utah data from transects D, H, and X (bioturbated sandstone and cross-bedded sandstone) by method of moments. Solid line has slope $\xi(1) = 0.26$ and broken line has slope $H = 0.21$.

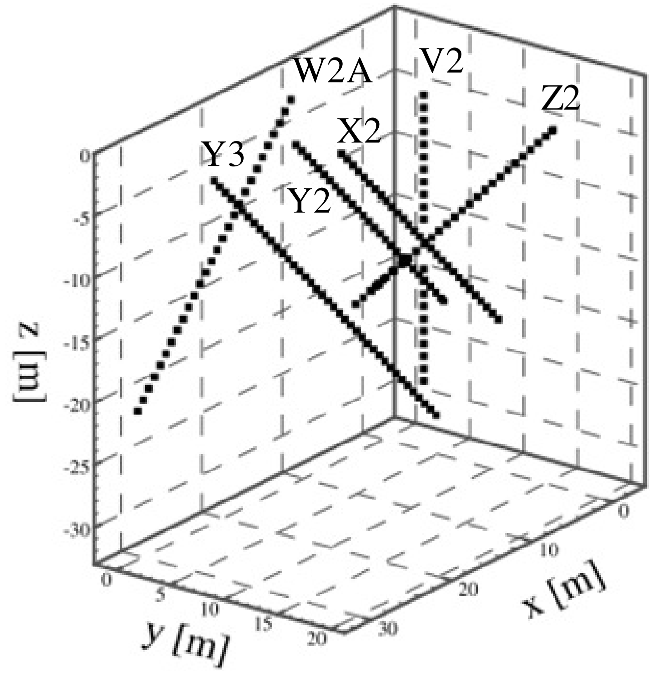

Fig. 1. Spatial locations along each borehole of Arizona data. Modified after Guzman et al. (1996).

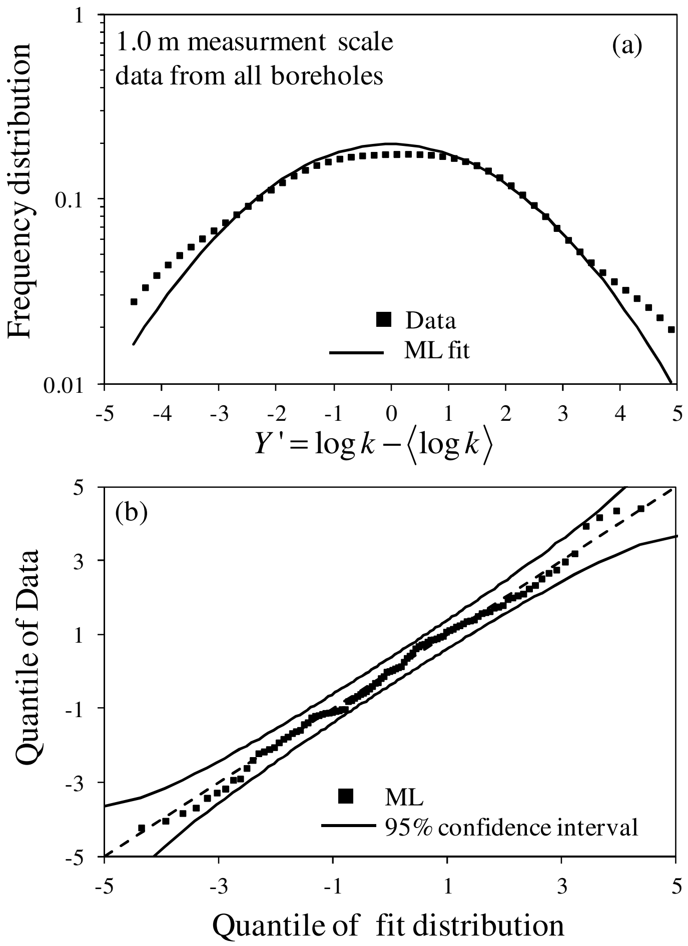

Fig. 2. (a) Frequency distribution (symbols) and ML estimated probability density function (solid curve) of Arizona data; (b) Q-Q plot of empirical data versus theoretical estimate of stable distribution.

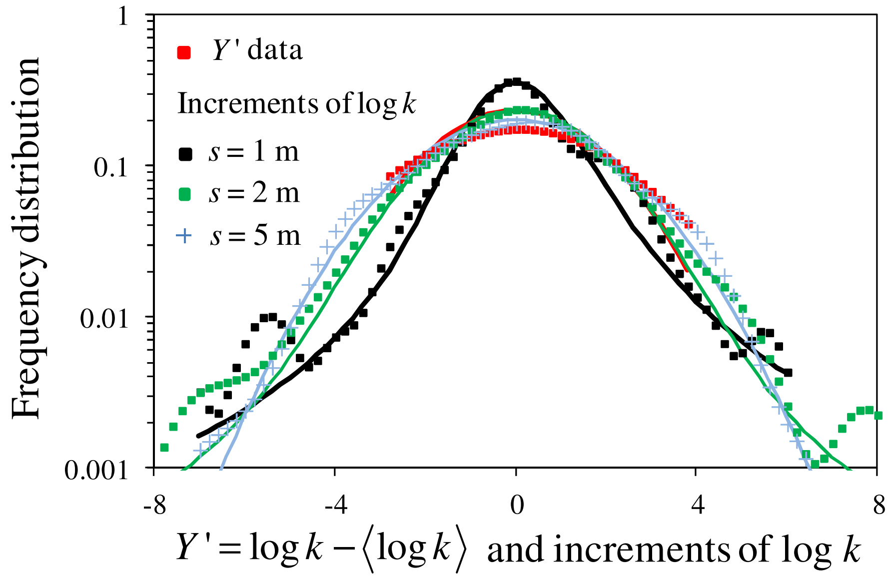

Fig. 3. Frequency distributions (symbols) and ML estimated probability density functions (curves) of Arizona $Y' = \log k - \langle \log k \rangle$ data (red) and log k increments at lags s = 1 m (black), 2 m (green), and 5 m (blue).

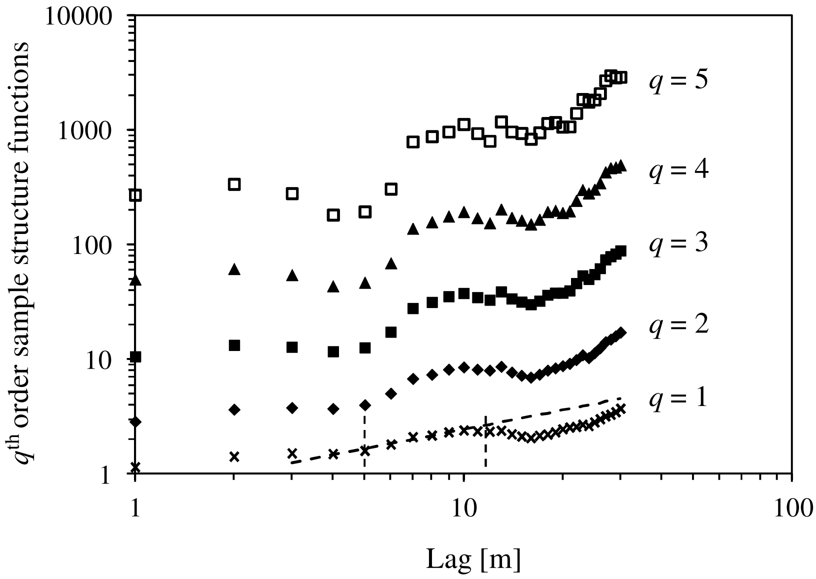

Fig. 4. Sample structure functions of orders q = 1, 2, 3, 4, 5 of Arizona data versus lag. Light vertical broken lines demarcate midrange of lags within which heavy inclined broken line, with slope taken to represent $\xi(1)$, was fitted to S_N^1.

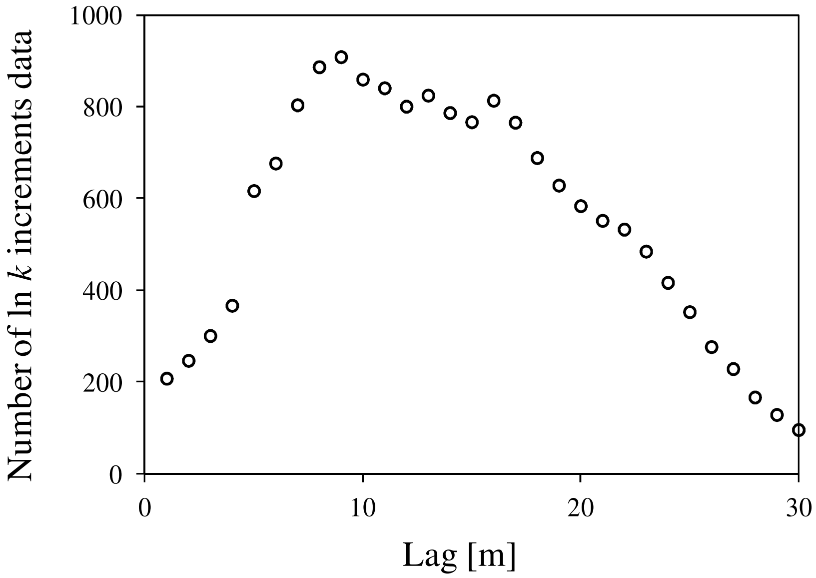

Fig. 5. Number of Arizona data pairs associated with each lag.

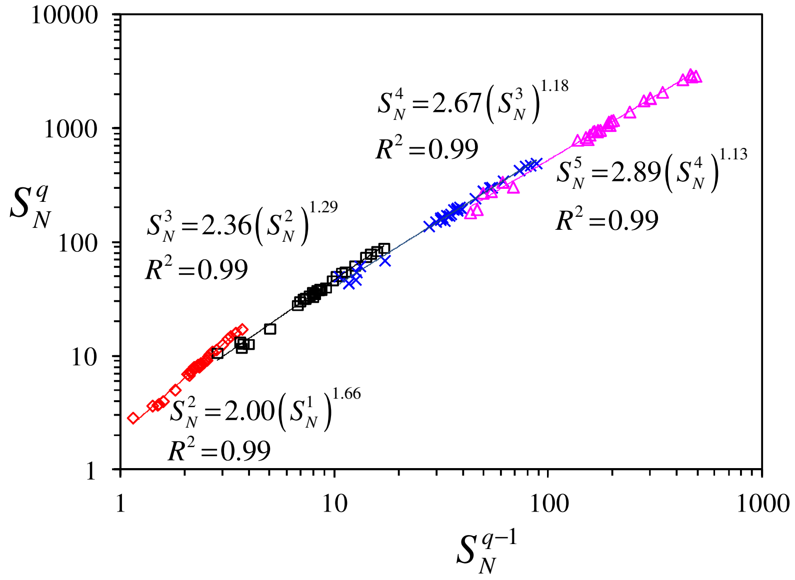

Fig. 6. Log-log variations of S_N^q of Arizona data with S_N^{q-1} for $2 \leq q \leq 5$. Solid lines represent indicated regression fits.

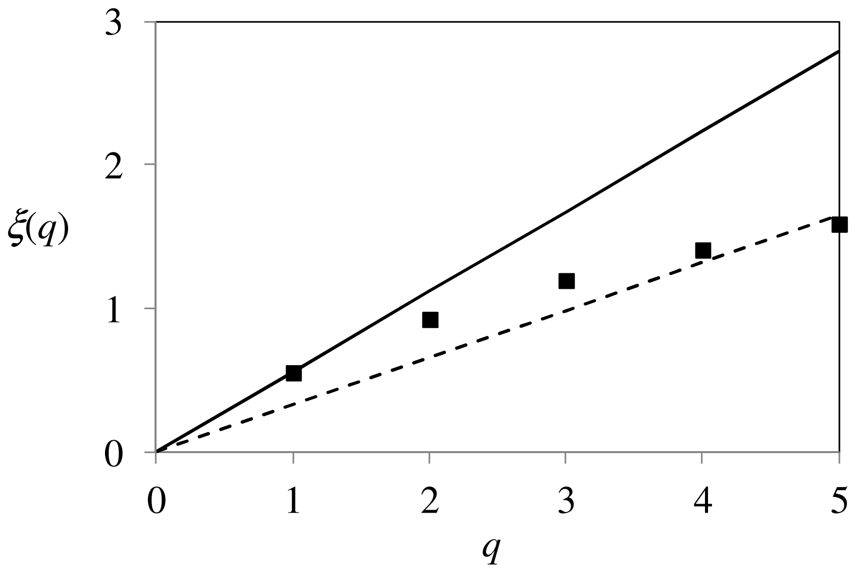

Fig. 7. $\xi(q)$ as a function of q (symbols) obtained via ESS based on $\xi(1) = 0.56$ computed for Arizona data by method of moments. Solid line has slope $\xi(1) = 0.56$ and dashed line slope $H = 0.33$ estimated for these data based on our theory, using maximum likelihood, by Riva et al. (2012).

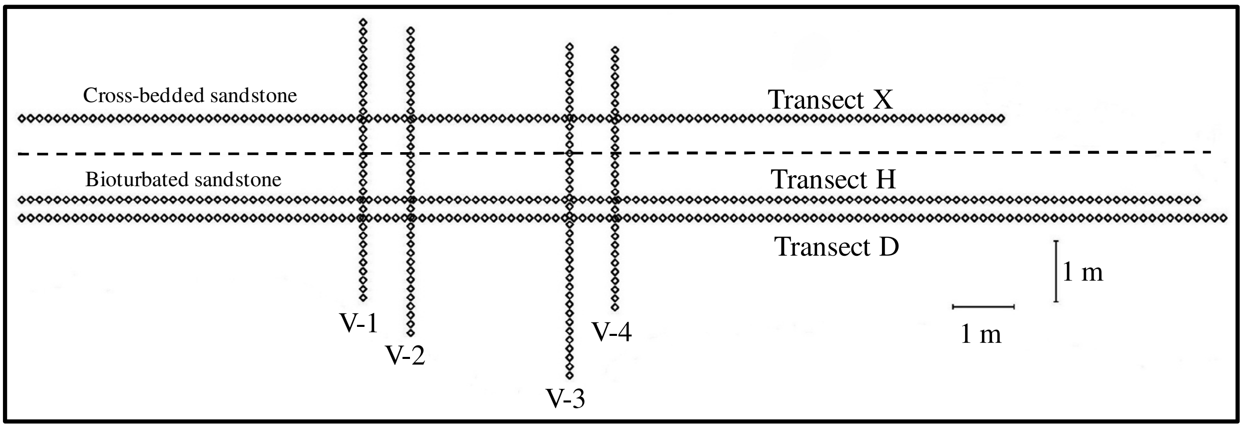

Fig. 8. Locations of nitrogen minipermeameter measurements along sandstone outcrop near Escalante, Utah. Modified after Castle et al. (2004).

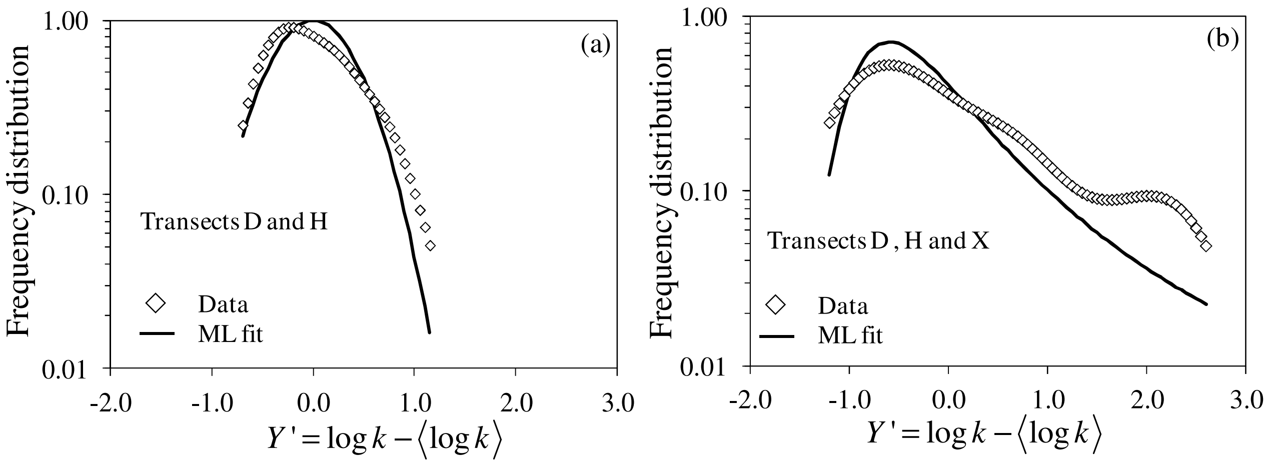

Fig. 9. Frequency distribution (symbols) and ML estimated probability density function (curves) of Utah $Y' = \log k - \langle \log k \rangle$ data on horizontal (a) transects D and H (bioturbated sandstone) and (b) transects D, H and X (bioturbated sandstone and cross-bedded sandstone).

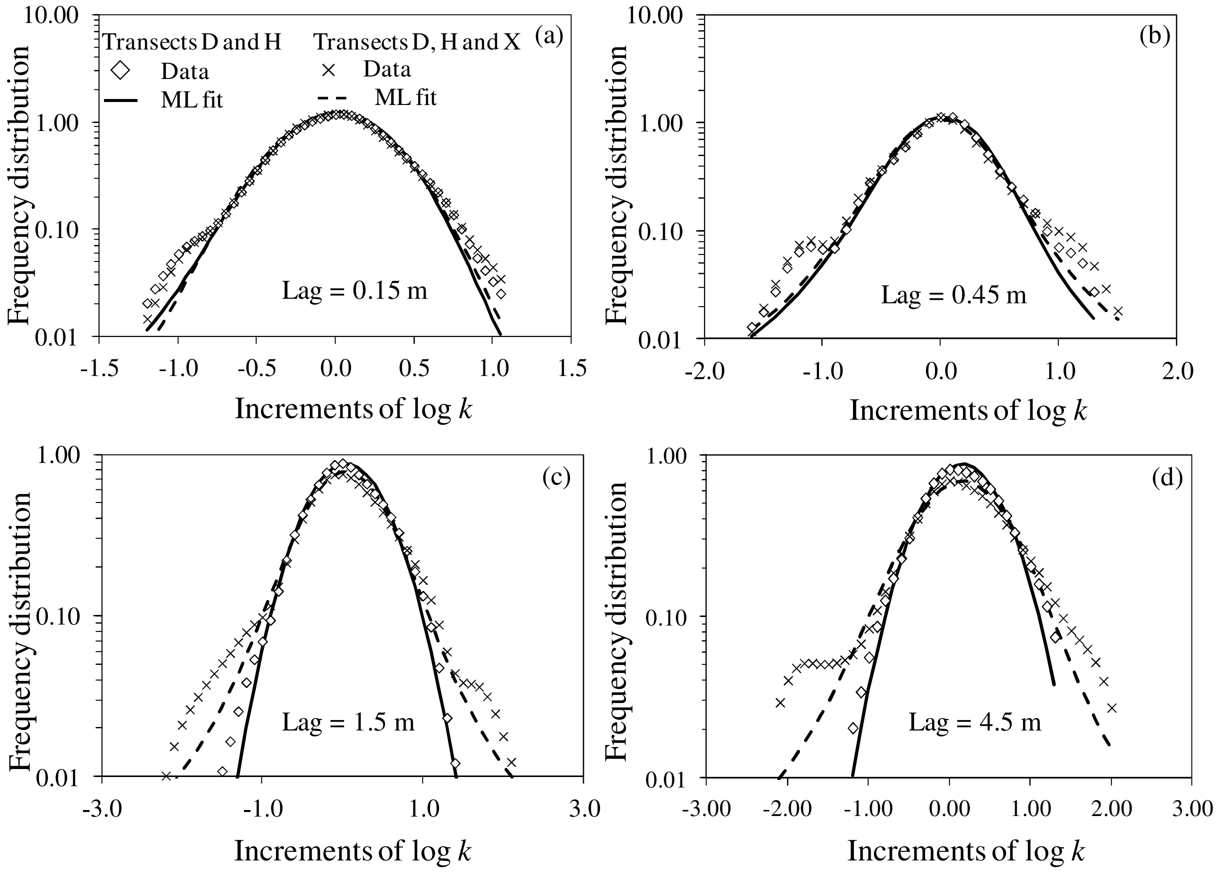

Fig. 10. Frequency distributions (symbols) and ML estimated probability density functions (curves) of Utah log k increments for transects D and H (bioturbated sandstone) and transects D, H and X (bioturbated sandstone and cross-bedded sandstone) at horizontal lags (a) 0.15 m, (b) 0.45 m, (c) 1.5 m, and (d) 4.5 m.

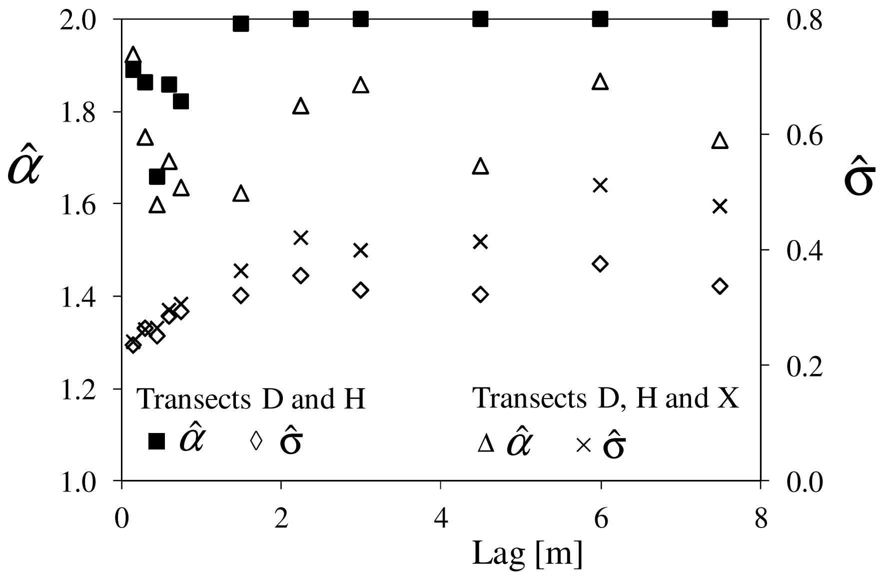

Fig. 11. Variations of ML Lévy index estimates $\hat{\alpha}$ and scale parameter estimates $\hat{\sigma}$ of Utah log permeability increments with horizontal lag for transects D and H (bioturbated sandstone) and transects D, H and X (bioturbated sandstone and cross-bedded sandstone).

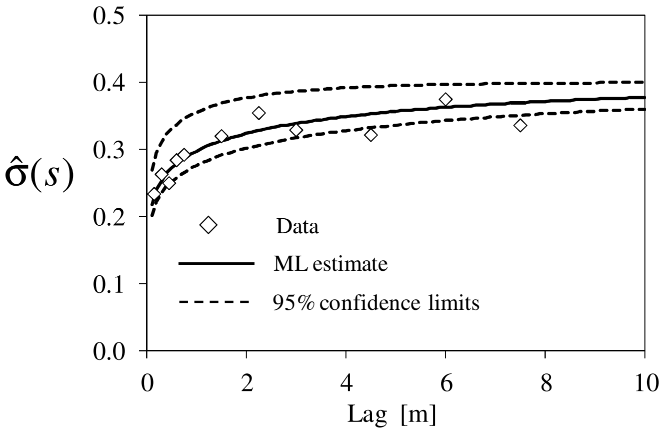

Fig. 12. Experimental scale parameter (diamonds) and their theoretical equivalents based on ML fit (solid curve) of TPV (6) based on data from transects D and H (bioturbated sandstone). Dashed curves represent 95% confidence limits of corresponding λ_u estimates.

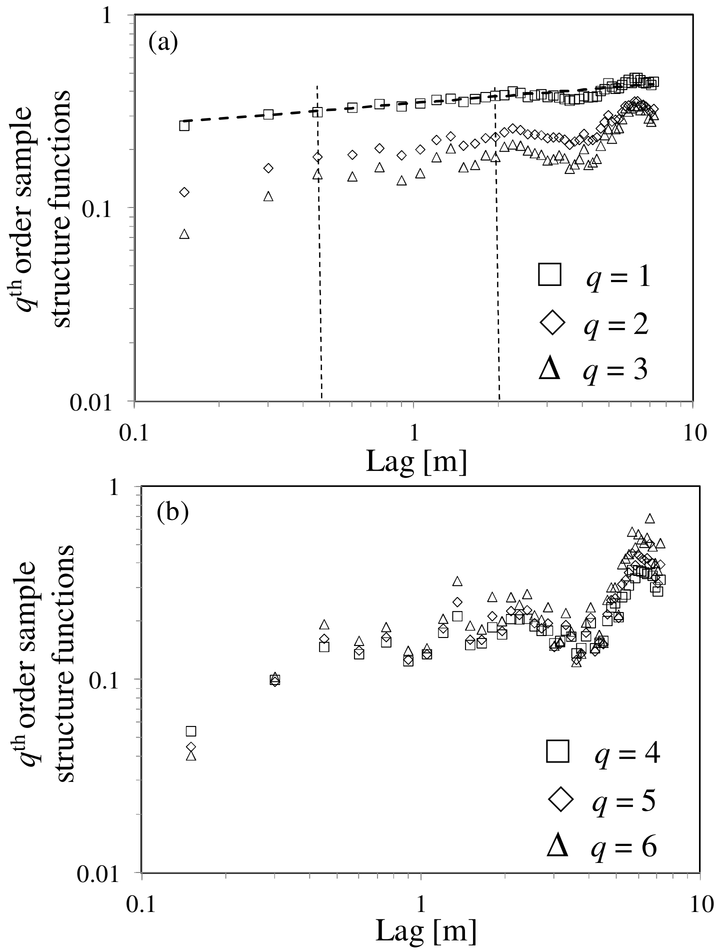

Fig. 13. Sample structure functions of order q = 1, 2, 3, 4, 5, 6 of Utah data from transects D and H (bioturbated sandstone). Light vertical broken lines demarcate midrange of lags within which heavy inclined broken line, with slope taken to represent $\xi(1)$, was fitted to S_N^1.

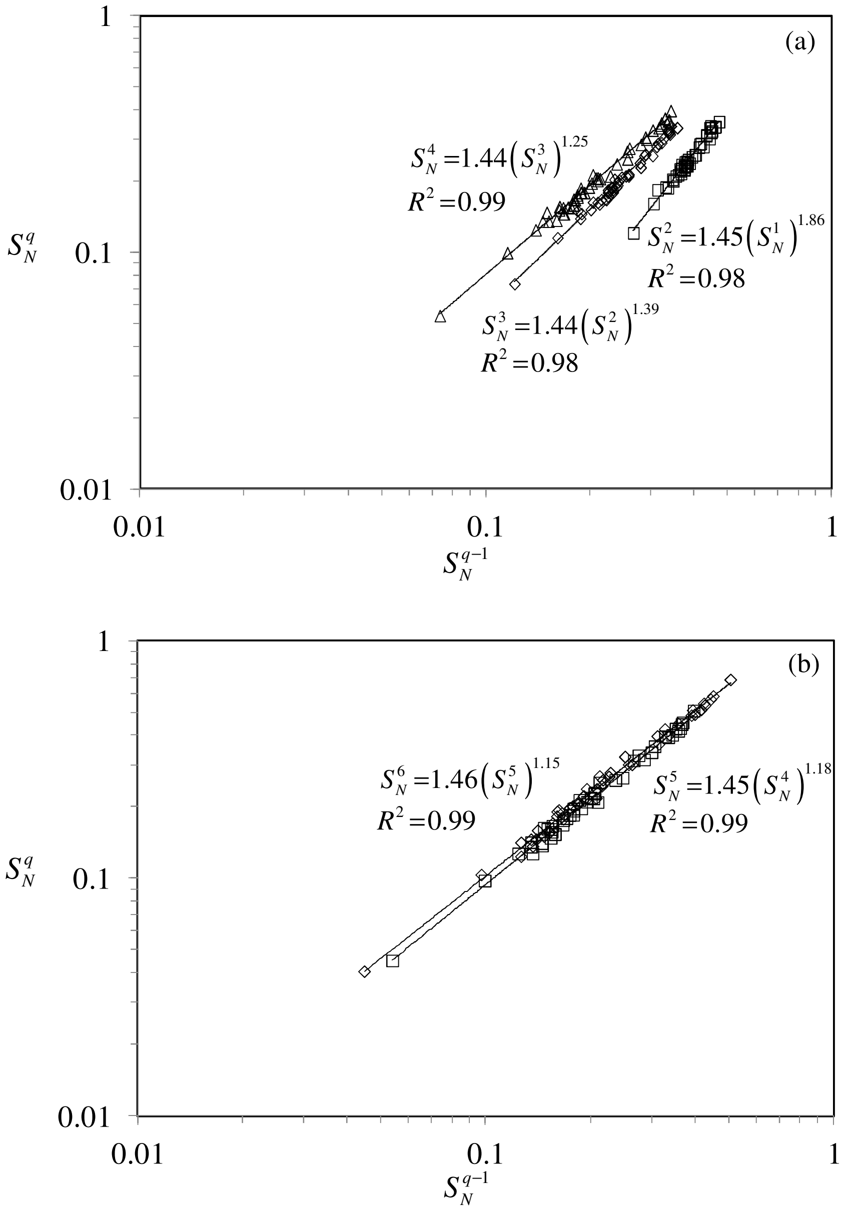

Fig. 14. Log-log variations of S_N^q of Utah data from transects D and H (bioturbated sandstone) with S_N^{q-1} for $2 \le q \le 6$. Solid lines represent indicated regression fits. Linear regression equations and related regression coefficients (R^2) are also reported.

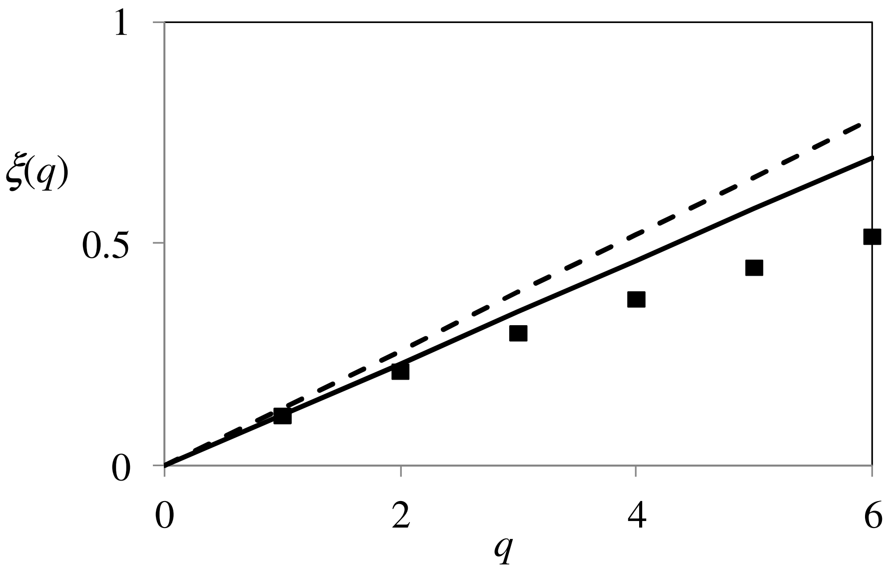

Fig. 15. $\xi(q)$ as a function of q (symbols) obtained via ESS based on $\xi(1) = 0.12$ computed for Utah data from transects D and H (bioturbated sandstone) by method of moments. Solid line has slope $\xi(1) = 0.12$ and broken line has slope $H = 0.13$.

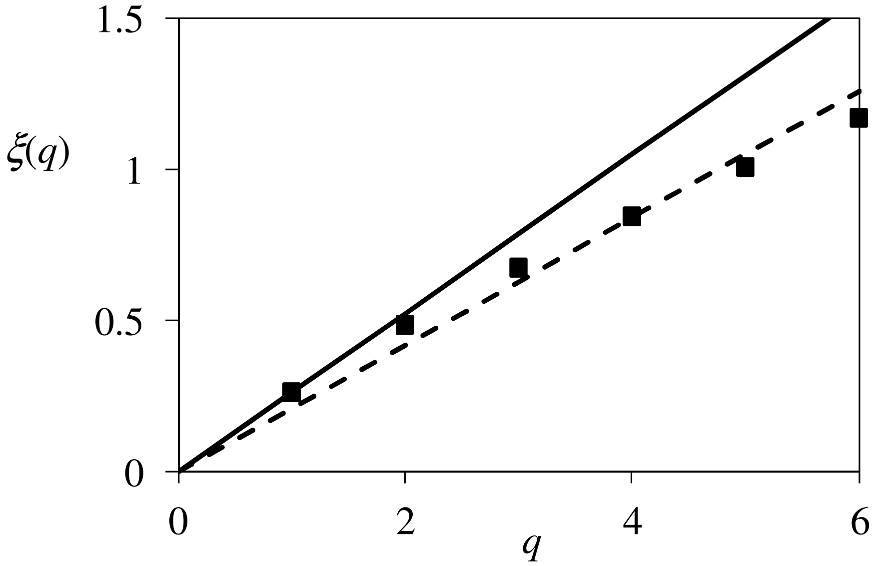

Fig. 16. $\xi(q)$ as a function of q (symbols) obtained via ESS based on $\xi(1)=0.26$ computed for Utah data from transects D, H, and X (bioturbated sandstone and cross-bedded sandstone) by method of moments. Solid line has slope $\xi(1)=0.26$ and broken line has slope $H = 0.21$.